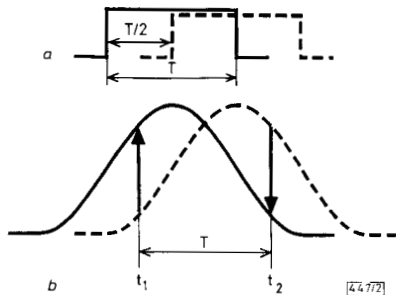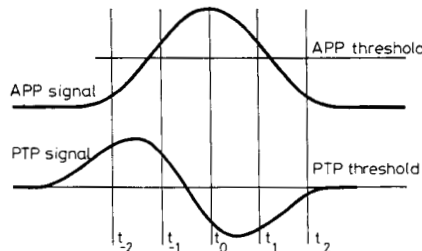As can be seen, the difference amplitude between the two filtered pulses has two maximum and opposite values at times t_1 and t_2 separated by T (upward and downward arrows in Fig. 2). Thus, a way to produce a PTP signal is to add the direct lowpass filtered received coded signal to the inverted signal delayed by T.

Fig. 2 *PTP signal*

  a Two overlapped pulses
  b Same pulses after lowpass filtering

The final decision is then taken according to the diagram in Fig. 3. At a decision time for a time slot, a pulse is considered to be present in this time slot only if the APP signal is higher than the APP threshold level and the PTP signal is lower than the PTP threshold level. Thus, in the example shown in Fig. 3, the pulse is first recognised in the time slot corresponding to t_0 that inhibits then the two next decisions corresponding to t_1 and t_2.

Fig. 3 *Decision diagram*

Clock recovery: One method for recovering the clock is to recognise, in the coded pulse stream, intervals between two pulses for which the first pulse is always in the same time slot. For example, in the EA signal in Fig. 1, when two pulses are separated by a duration = 3 time slots, the first is always in slot 2.

When this method is not applicable, as for example in the case of EB signal in Fig. 1, it is then possible to recover $4F$ (F = clock frequency) from the coded signal and to synchronise the division by 4 according to the result of a mean count of pulses per slot, the mean occurrence frequency being different for each binary pattern used. Another way for this example is to transmit extra pulses in unauthorised time slots especially for clock recovery purposes.

Experimental results and conclusion: A feasibility experiment with $n = 2$ and 10, 11 has been performed at a rate of 140 Mbit/s in an electrical loop configuration. The error probabilities concerning PTP and APP signal decisions were quasi-identical in a white noise condition with a pulse duration equal to the bit duration (for this particular case, extra PTP signals are needed to achieve nondegraded decisions when two pulses are separated by $3T/2$). The sensitivity improvement over NRZ was slightly better than the ratio in mean number of transmitted pulses (1·8 dB), because the bandwidth resulting of optimal filtering before decision is smaller for both APP and PTP signals than for NRZ signal.

An experiment in a 140 Mbit/s, 1·55 μm direct-detection optical transmission system exhibiting a sensitivity better than 200 photons/bit has also been conducted and will be the subject of a further paper.

L. POPHILLAT   *24th October 1990*

CNET, BP40, Route de Trégastel
22301 Lannion, France

References

1 XIANDA, D., ENGLEFIELD, C. G., GOUD, P. A., and RAZDAN, R.: 'Four-level pulse width modulation for fiber optic communications', *IEEE Trans.*, 1982, **COM-30**, pp. 1958–1963
2 GARRETT, I.: 'Pulse-position modulation for transmission over optical fibers with direct or heterodyne detection', *IEEE Trans.*, 1983, **COM-31**, pp. 518–527
3 SUGIYAMA, H., and NOSU, K.: 'MPPM: a method for improving the band-utilization efficiency in optical PPM', *J. Lightwave Technol.*, 1989, **7**, pp. 465–472
4 KASPER, B. L., and CAMPBELL, J. C.: 'Multigigabit-per-second avalanche photodiode lightwave receivers', *J. Lightwave Technol.*, 1987, **5**, pp. 1351–1364
5 BAR-DAVID, I., and KAPLAN, G.: 'Information rates of photon-limited overlapping pulse position modulation channels', *IEEE Trans.*, 1984, **IT-30**, pp. 455–464
6 POPHILLAT, L.: 'Video transmission using a 1·3 μm LED and monomode fibre'. Proceedings of 10th ECOC, Stuttgart, September 1984, pp. 238–239
7 HEATLEY, D. J.: 'SNR comparison between two designs of PFM demodulator used to demodulate PFM or FM', *Electron. Lett.*, 1985, **21**, pp. 214–215
8 ABSHIRE, J. B.: 'Performance of OOK and low-order PPM modulations in optical communications when using APD-based receivers', *IEEE Trans.*, 1984, **COM-32**, pp. 1140–1143

GALLIUM ARSENIDE PSEUDO-CURRENT-MODE LOGIC

Indexing terms: Logic devices, Semiconductor devices

A new GaAs logic style is proposed, one which uses current as the signal processing parameter. Built around a current mirror, this direct-coupled FET logic (DCFL) analogue, dubbed pseudo-current-mode logic (PCML), features a power-delay product of 83 fJ and rail-to-rail logic swing.

Introduction: A number of approaches exist for the design of GaAs logic circuits. One of the more attractive is DCFL whose circuit simplicity and low power-delay product are well suited to implementing GaAs LSI. A drawback of this approach, however, is its small logic swing, restricted to 0·6 V, and correspondingly low noise margins, resulting from conduction of the Schottky-gate diodes.[1] The effect of low noise margins is further exacerbated by the low intrinsic gain ($g_m r_o$) of the devices which results in a low-gain circuit.

The low noise margins encountered in DCFL circuits impose stringent requirements on threshold uniformity and process variation of the enhancement-mode devices. This fact has spurred an interest in topologies that increase the logic swing or alleviate strict process requirements altogether. One such approach is source-coupled FET logic (SCFL),[2,3] which is insensitive to threshold variations. Here we present another, a new circuit which is a DCFL analogue, but capable of rail-to-rail output swings.

Pseudo-current-mode logic: The proposed pseudo-current-mode logic inverter is shown in Fig. 1. With reference to the circuit of Fig. 1, the operation can be qualitatively described as follows:

Transistor J1 functions as a voltage-to-current convertor and sources current to the current mirror formed by J2–J4 when the input goes high, causing the output node to be pulled down. When the input goes low the pull-down current is disrupted, and J5 drives the output up to the supply. Transistor J3 serves to discharge the internal node and so ensures

the turn off of J4 when the input goes low, as well as acting as a simple design variable in adjusting the inverter's switching threshold.
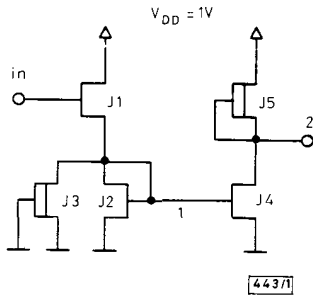

Fig. 1 *Pseudo-current-mode logic inverter*

This circuit comes with the usual amenities of current-mode signal processing. For example, the internal node in Fig. 1 is a low impedance node with correspondingly small voltage swing. This reduces the effect of voltage slewing there, suggesting the potential for high-speed performance. In addition, the circuit is built around a current mirror with the advantage of low-voltage operation. Though a 1·0 V supply was chosen for DCFL compatibility, unlike DCFL, this circuit is capable of rail-to-rail output swings.

As is the case for DCFL, PCML is a ratioed design that is reminiscent of NMOS and grounded-gate PMOS. Device sizes are usually chosen so that the output can be pulled down to a conveniently low logic-zero voltage. Using the classic square-law FET equation, we can obtain the grossly approximate relationship between the output devices as

$$\frac{W_D}{W_E} \approx \frac{\beta_E}{\beta_D} \left[\frac{2(V_G - V_{Te})V_o - V_o^2}{V_{Td}^2} \right]$$

where V_G is the maximum gate voltage of the output enhancement-mode device. This relation comes about as a result of J4 entering the triode region as J4 output approaches ground, thus disabling current mirror action. Thereafter, it functions as a nonlinear resistor. For TriQuint's 1 μm GaAs E/D process,[4] and $V_{o, max} = V_{Te}$, the ratio W_D/W_E turns out to be 0·27. Device sizes for a design that results in equal noise margins are as follows:

$$w1 = 25 \,\mu m$$

$$w2 = w4 = 15 \,\mu m$$

$$w3 = w5 = 3 \,\mu m$$

This circuit was simulated using Hspice and the resulting transfer characteristic and transient response, when driven at 800 MHz from a source with a 5·0 kΩ output resistance, are shown in Fig. 2. In addition, the output of a nine-inverter ring oscillator is shown in Fig. 3. The circuit's performance for a fanout of one is summarised in Table 1.

PCML gate design: The basic inverter of Fig. 1 can be easily modified to create NOR and NAND gates as illustrated in Fig. 4. The close topological relationship of the NOR to the inverter suggests comparable speed performance, whereas the NAND, with its series input chain, should be marginally slower. To verify gate operation, a two-input NOR gate was simulated yielding a propagation delay of 330 ps for a fan-out of two. This compares well with the results obtained for the inverter; a 100% increase in load capacitance resulted in only a 30% increase in propagation time.

Table 1 PERFORMANCE OF PCML INVERTER

Noise margins		Propagation delay	Power consumption per gate	Power-delay product
NM_L	NM_H			
V	V	ps	mW	fJ
0·36	0·36	250	0·33	82·5

In spite of its first-order acceptability, the NAND realisation was abandoned for general circuits because of gate conduction of the input transistors, a phenomenon that is welcome in synthesising the inverter and the NOR. In particular, with A = 0 and B = 1, gate conduction of J1b causes the output to be pulled down because of the large forward bias on the gate diode. Nevertheless, the NAND can be used in front-end applications where input signals are typically small.
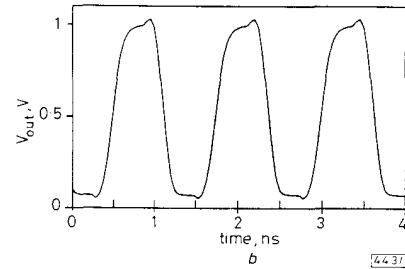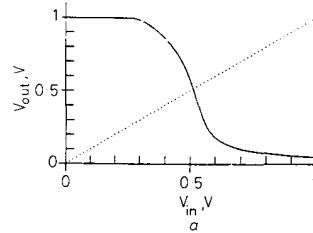

Fig. 2 *PCML transfer characteristic and transient response*

a Transfer characteristic
b Transient response at 800 MHz

To further highlight the potential of PCML, the supply in Fig. 1 was increased to 2·5 V to obtain BFL-comparable logic swings. As before, the circuit was optimised for nearly equal noise margins; the device sizes that resulted in $NM_L = 0·7$ V and $NM_H = 1·0$ V are as follows:

$$w1 = 8 \,\mu m$$

$$w2 = w4 = 20 \,\mu m$$

$$w3 = 15 \,\mu m$$
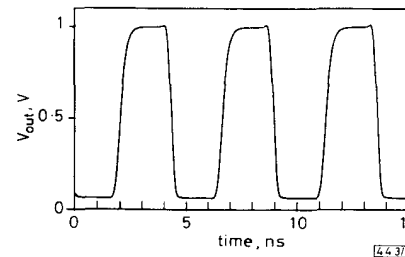
$$w5 = 5 \,\mu m$$

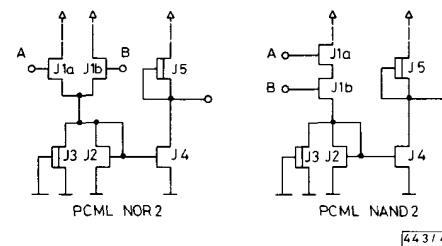Fig. 3 *Ring oscillator output (employing 9 inverting stages)*

Fig. 4 *PCML NOR and NAND*

A ring-oscillator simulation resulted in a gate propagation delay of 135 ps with 1·5 mW consumption per gate. This power-delay product is superior to that obtained from BFL circuits.

Conclusion: A DCFL analogue called pseudo-current-mode logic has been presented that combines the design simplicity of DCFL with current-mode signal processing to produce a circuit which is more immune from noise than DCFL. The larger logic swing and noise margins (0·36 V) as compared to DCFL is an important advantage for the design of GaAs LSI. As with DCFL, however, the circuit suffers from poor functionality.

R. A. DUNCAN   23rd October 1990
K. C. SMITH
A. S. SEDRA

Department of Electrical Engineering
University of Toronto
Toronto, Ontario M5S 1A4, Canada

References

1 LONG, S. I., and BUTNER, S. E.: 'Gallium arsenide digital integrated circuit design' (McGraw-Hill, 1990), pp. 210–216
2 KATSU, S., NAMBU, S., SHIMANO, A., and KANO, G.: 'A source coupled FET logic—a new current-mode approach to GaAs logics', *IEEE Trans.*, 1985, **ED-32**, pp. 1114–1118
3 TAMURA, A., *et al.*: 'High-speed GaAs SCFL divider', *Electron. Lett.*, July 1985, **21**, pp. 605–606
4 'TriQuint QED/A Design Manual' (TriQuint Semiconductor, Beaverton, OR., USA, 1989)

A STEP TOWARDS DETERMINING TRANSIENT RESPONSE OF CHIRAL MATERIALS: KRAMERS–KRONIG RELATIONS FOR CHIRAL PARAMETERS

Indexing terms: Transients, Radar cross-sections, Dielectrics

The Kramers–Kronig relations for the chirality admittance of isotropic reciprocal chiral materials are given using the techniques applied for linear, spatially local and causal operators. The results provide a physical insight into the analysis of electromagnetic pulse propagation in chiral materials. Such analysis will find potential applications in the design of broadband chiral materials in pulsed radar environments and the wideband control and management of radar cross-section of chiral coated targets.

Chiral materials, commonly known as optically active materials in the optical regime, have attained renewed interest in recent years owing to the possibility of constructing such materials in the microwave and millimetre-wave regimes.[1] It has been shown that the handedness property of these media leads to the design of a variety of novel devices in the microwave, millimetre-wave and optical domains.[2-4] In the frequency domain, a chiral material is electromagnetically characterised by the following set of constitutive relations

$$\tilde{D} = \varepsilon_c(\omega)\tilde{E} + i\xi_c(\omega)\tilde{B}$$
$$\tilde{H} = \tilde{B}/\mu_c(\omega) + i\xi_c(\omega)\tilde{E} \qquad (1)$$

where $\tilde{D}$, $\tilde{E}$, $\tilde{B}$, and $\tilde{H}$ are the usual time-harmonic ($e^{-i\omega t}$) electromagnetic field vectors in the frequency domain, $\varepsilon_c(\omega)$, $\mu_c(\omega)$, and $\xi_c(\omega)$ are the permittivity, permeability, and chirality admittance of the medium, respectively. Several fundamental problems of monochromatic electromagnetic wave propagation in such media have been studied in detail.[2-5] However, to date, less attention has been paid to the interaction of nonsinusoidal electromagnetic pulses with chiral media, or the time domain analysis of these media. In this letter, the first step is made towards understanding the transient response of chiral materials. More specifically, we analyse certain characteristics of the chirality admittance ξ_c and we present the Kramers–Kronig relations for this parameter. The results obtained from this study have helped us analyse the time-domain response of chiral materials.

The relationships among $\tilde{E}$, $\tilde{B}$, $\tilde{D}$ and $\tilde{H}$ given in eqn. 1 are taken to be linear, spatially local and causal. In addition, it is assumed, on physical grounds, that the medium be stable, i.e. for finite values of $\tilde{E}$ and $\tilde{B}$, resulting $\tilde{D}$ and $\tilde{H}$ must also be finite. Similar to the case of material permittivity given in the literature,[6] the properties of linearity, causality, and stability suggest some relations between the real and imaginary parts of the chirality admittance ξ_c in the frequency domain. To develop such relations, it is important to consider the linear and causal nature of eqn. 1 and write it in the time domain. The most general form of these linear relations can be given as

$$D(t) = \varepsilon_0 E(t) + \int_0^\infty F_c(\tau)E(t-\tau)\,d\tau + \int_0^\infty C_c(\tau)B(t-\tau)\,d\tau$$

$$H(t) = (1/\mu_0)B(t) + \int_0^\infty G_c(\tau)B(t-\tau)\,d\tau + \int_0^\infty C_c(\tau)E(t-\tau)\,d\tau \quad (2)$$

where $D(t)$, $E(t)$, $B(t)$, and $H(t)$ are the electromagnetic field vectors in the time domain. Here $F_c(t)$, $G_c(t)$, and $C_c(t)$ are real functions of time, and they represent electric, magnetic, and chiral susceptibility kernels or impulse responses that depend on the specific type of chiral medium. As the above relations are to be causal, $F_c(t)$, $G_c(t)$, and $C_c(t)$ are zero for $t < 0$, and hence the lower limits of the integrals in eqn. 2 are zero. The properties of kernels $F_c(t)$ and $G_c(t)$ have been studied and treated elsewhere.[6,7] The chiral terms in eqn. 2 and the kernel $C_c(t)$ are of interest here. They represent the cross coupling between electric and magnetic effects in chiral media. For short hand, we denote these two integrals by $D_c(t)$ and $H_c(t)$, i.e.

$$D_c(t) = \int_0^\infty C_c(\tau)B(t-\tau)\,d\tau$$

$$H_c(t) = \int_0^\infty C_c(\tau)E(t-\tau)\,d\tau \qquad (3)$$

If $B(t)$ and $E(t)$ are finite, then the integrals given in eqn. 3 must result in finite $D_c(t)$ and $H_c(t)$. This requires that $C_c(t)$ be absolutely integrable,[8] i.e. $\int_0^\infty |C_c(t)|\,dt < \infty$. Transforming eqns. 3 into the Fourier domain and then comparing the outcome with eqn. 1, we find that

$$\xi_c(\omega) = -i \int_0^\infty C_c(t)\exp(i\omega t)\,dt \qquad (4)$$

The chirality admittance is in general a complex quantity with real and imaginary parts denoted by ξ_c' and ξ_c'', i.e. $\xi_c(\omega) = \xi_c'(\omega) + i\xi_c''(\omega)$. Following a similar method used for a general susceptibility,[6] certain characteristics of $\xi_c(\omega)$ as a function of frequency may now be ascertained by considering restrictions imposed on $C_c(t)$. Because $C_c(t)$ is a real function, from eqn. 4, we find that $\xi_c^*(\omega) = -\xi_c(-\omega^*)$ where ω is the complex frequency given by $\omega = \omega' + i\omega''$. From this relation, we find that for purely imaginary frequency, $\xi_c^*(i\omega'') = -\xi_c(i\omega'')$ which implies that the function $\xi_c(\omega)$ is purely imaginary on the imaginary frequency axis. If the frequency is taken to be real, i.e. $\omega'' = 0$, the following relations are obtained for the real and imaginary parts of $\xi_c(\omega)$:

$$\xi_c'(\omega') = -\xi_c'(-\omega')$$
$$\xi_c''(\omega') = \xi_c''(-\omega') \qquad (5)$$